Electronic Supplementary Material (ESI) for RSC Advances.

Supporting information for

Super-robust Superamphiphobic Surface with Anti-icing Property

Huanhuan Wang, Haitao Lu, Xia Zhang*

National & Local Joint Engineering Research Center for Applied Technology of Hybrid

Nanomaterials, Henan University, Kaifeng 475004, PR China. Email: xia.zhang@ucl.ac.uk

Fig. S1. A superhydrophobic surfaces under liquid paraffin with contact angle about 174 ±1°.

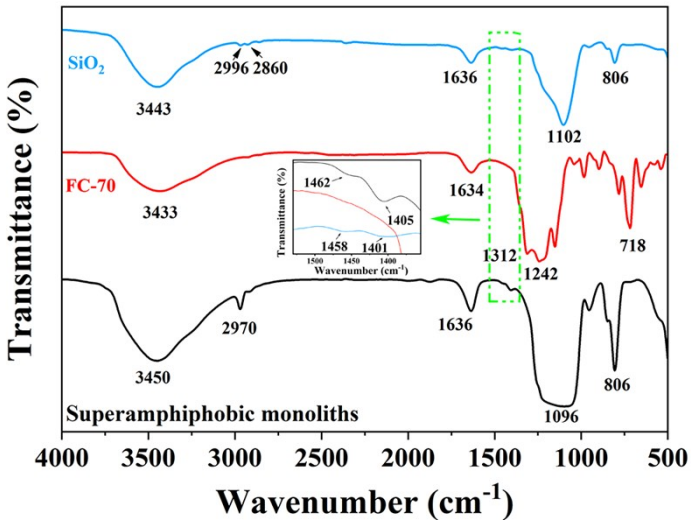

Fig. S2. FT-IR spectra of nano-SiO_2, FC-70 and superamphiphobic monoliths.

FT-IR analysis was conducted to investigate the structure of nano-SiO_2, FC-70 and superamphiphobic monoliths. The nano-SiO_2 shows the absorbance peaks at 3443 cm^{-1} and 1636 cm^{-1}, and these absorbance peaks correspond to the asymmetric stretching vibration and blending stretching vibration of -OH, respectively. The absorbance peaks at 2996 cm^{-1} and 2860 cm^{-1} are assigned to the asymmetric stretching vibration of -CH_3, and the double peaks at 1458 cm^{-1} and 1401 cm^{-1} can be attributed to the deformation vibration of saturated C-H, respectively [S1]. Those at 1102 cm^{-1} and 806 cm^{-1} are attributed to the asymmetric stretching vibration and symmetric stretching vibration of Si-O-Si. This indicates that the hydrophobic group -CH_3 was successfully modified on the surface of nano-SiO_2. FC-70 (perfluorotripentylamine) shows extremely strong absorption peaks at 1312 cm^{-1}, 1242 cm^{-1} and 1152 cm^{-1}, which are attributed to the stretching vibration peaks of -CF_3 and -CF_2 [S2]. Comparing these three infrared curves, the superamphiphobic monoliths showed obvious absorption at the characteristic absorption peak positions of SiO_2 and FC-70, and the peak intensity increased at the common absorption peak position of the two, so it can be considered that the infrared curve of superamphiphobic monoliths is superimposed by the spectral lines of SiO_2 and FC-70.

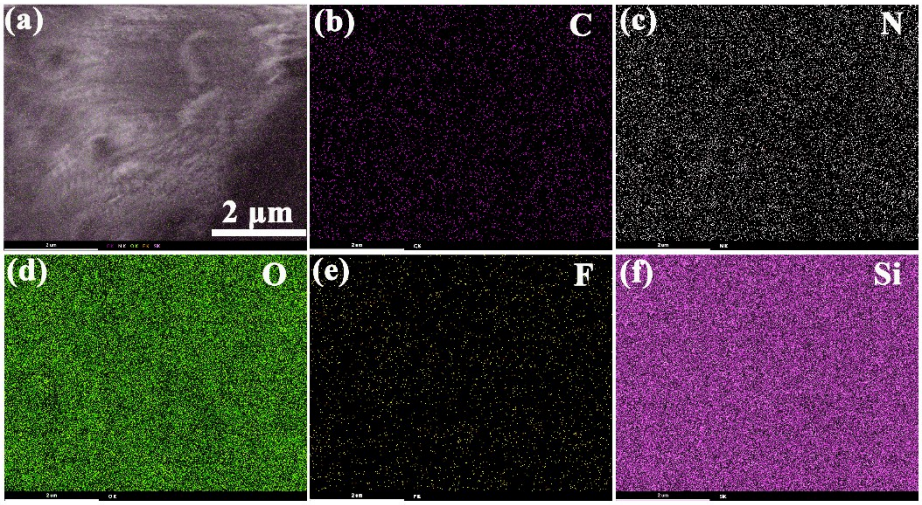

Fig. S3. Element distribution maps of the superamphiphobic monoliths.

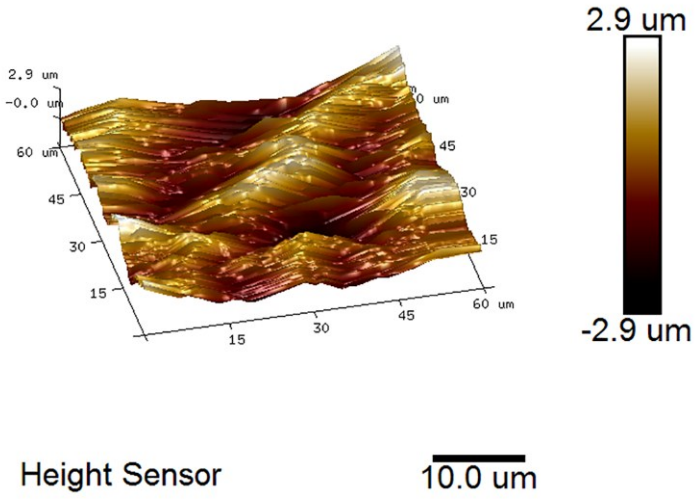

Fig. S4. AFM images of the superamphiphobic monoliths. The average of outline arithmetic mean deviation (Ra) was 1.362 μm.

To further determine the surface roughness of superamphiphobic monoliths, the AFM was investigated with a scanning area of 60 μm. The three-dimensional appearance of the surface of superamphiphobic monoliths was detected by atomic force microscopy (AFM, Dimension Icon, Bruker). The streaks and pits on the surface in the AFM images are traces of the remaining marks that have been sanded by sandpaper. The average of outline arithmetic mean deviation (Ra) micro-roughness for the superamphiphobic monoliths was 1.362 μm.

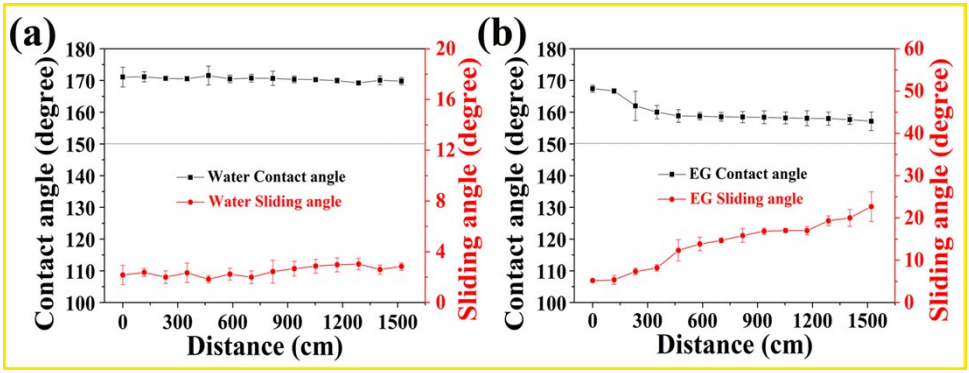

Fig. S5. Relationship between contact angle, sliding angle and abrasion distance. (a) Water and (b) ethylene glycol.

Table S1. Classification system for radar diagram.

Radar diagram point	**CA α [deg]**	**SA β [deg]**
1	$\alpha < 130$	$\beta > 35$
2	$130 \leq \alpha < 135$	$30 < \beta \leq 35$
3	$135 \leq \alpha < 140$	$25 < \beta \leq 30$
4	$140 \leq \alpha < 145$	$20 < \beta \leq 25$
5	$145 \leq \alpha < 150$	$16 < \beta \leq 20$
6	$150 \leq \alpha < 155$	$12 < \beta \leq 16$
7	$155 \leq \alpha < 160$	$8 < \beta \leq 12$
8	$160 \leq \alpha < 165$	$4 < \beta \leq 8$
9	$165 \leq \alpha < 170$	$1 < \beta \leq 4$
10	$\alpha \geq 170$	$\beta \leq 1$

Table S2. Average values and errors of performance characteristics and their corresponding points on radar diagram.

Priority	**Angle γ [deg]**
WCA initial	171.4±1.5 (10)
WSA initial	2.2±0.8 (9)
WCA after abrasion	169.8±1.1 (9)
WSA after abrasion	2.8±0.3 (9)
EGCA initial	167.4±1.1 (9)
EGSA initial	5.2±0.3 (8)
EGCA after abrasion	157.2±2.9 (7)
EGSA after abrasion	22.7±3.5 (4)
WCA pH=1	169.8±2.6 (9)
WCA pH=14	153.4±1.7 (6)
EGCA pH=1	158.9±1.4 (7)
EGCA pH=14	154.9±2.1 (6)

Supporting Videos

Video S1 and S2
Water and ethylene glycol droplets bouncing on the superamphiphobic block surface.

Video S3
The monolith demonstrates superhydrophobicity under oil.

Video S4 and S5
The obtained monoliths were dipped and then removed from blood and mud to test their liquid and earth repellence.

Video S6
Dust was easily removed by water on superamphiphobic monolith surface.

Video S7
Melting process of ice droplets on glass and monolith surface at room temperature.

Video S8
De-icing test by tapping the hydrophilic glass and superamphiphobic monolith surfaces.

References
[S1] J. Liu, Y. Cheng, K. Xu, L.L. An, Y.H. Su, X.H. Li, Z.J. Zhang, Effect of nano-silica filler on microstructure and mechanical properties of polydimethylsiloxane-based nanocomposites prepared by "inhibition-grafting" method, Compos. Sci. Technol. 167 (2018) 355-363, https://doi.org/10.1016/j.compscitech.2018.08.014.
[S2] J.C. Yang, H.B. Ni, J. Li, C.X. Zhao and Y.M. Zhang, Synthesis and characterisation of p-perfluoro{-1-[2-(2-fluorosulfonylethoxy)propoxy]} ethylated polystyrene, J. Chem. Res. 8 (2005) 546-548, https://doi.org/10.3184/030823405774663336.